

Collagen-Tannic Acid Spheroids for β -Cell Encapsulation Fabricated Using a 3D Bioprinter

Laura Clua-Ferré, Francesco De Chiara, Júlia Rodríguez-Comas, Jordi Comelles, Elena Martínez, Amelie Luise Godeau, Ainhoa García-Alamán, Rosa Gasa, and Javier Ramón-Azcón*

Type 1 Diabetes results from autoimmune response elicited against β -cell antigens. Nowadays, insulin injections remain the leading therapeutic option. However, injection treatment fails to emulate the highly dynamic insulin release that β -cells provide. 3D cell-laden microspheres have been proposed during the last years as a major platform for bioengineering insulin-secreting constructs for tissue graft implantation and a model for in vitro drug screening platforms. Current microsphere fabrication technologies have several drawbacks: the need for an oil phase containing surfactants, diameter inconsistency of the microspheres, and high time-consuming processes. These technologies have widely used alginate for its rapid gelation, high processability, and low cost. However, its low biocompatible properties do not provide effective cell attachment. This study proposes a high-throughput methodology using a 3D bioprinter that employs an ECM-like microenvironment for effective cell-laden microsphere production to overcome these limitations. Crosslinking the resulting microspheres with tannic acid prevents collagenase degradation and enhances spherical structural consistency while allowing the diffusion of nutrients and oxygen. The approach allows customization of microsphere diameter with extremely low variability. In conclusion, a novel bio-printing procedure is developed to fabricate large amounts of reproducible microspheres capable of secreting insulin in response to extracellular glucose stimuli.


β -cell destruction, which leads to persistent high blood glucose levels.^[1] Currently, a therapy based on daily exogenous insulin administration is the primary treatment for patients with T1DM. However, this temporal treatment does not mimic the real-time insulin secretion of β -cells resulting in loss of capacity to control glucose homeostasis and leading to chronic complications such as cardiovascular diseases, nephropathy, and retinopathy.^[2] Nowadays, islet transplantation combined with immunosuppressive drugs is a promising way to provide new β -cells to diabetic patients.^[3] However, several drawbacks limit its exploitation in the clinical fields, such as the scarcity of compatible cadaveric donors, the requirement of immunosuppressors, and the islet loss due to the lack of vascularization and oxygenation.^[4] Another common drawback of direct infusion of insulin-secreting cells is the poor retention of cells following implantation. One solution to cellular retention at the injection site has been the use of biomaterials to encapsulate cells within a microenvironment before implantation.^[5] In this line, encapsulation of beta-cells within protective semipermeable biomaterials has emerged to overcome the challenges posed by islet transplantation. The biocompatible cell-laden material then should have

1. Introduction

Type 1 Diabetes Mellitus (T1DM) is an autoimmune disease characterized by an insulin deficiency caused by pancreatic

environment before implantation.^[5] In this line, encapsulation of beta-cells within protective semipermeable biomaterials has emerged to overcome the challenges posed by islet transplantation. The biocompatible cell-laden material then should have

L. Clua-Ferré, F. De Chiara, J. Rodríguez-Comas, J. Comelles, E. Martínez, A. L. Godeau, J. Ramón-Azcón
Institute for Bioengineering of Catalonia (IBEC)
The Barcelona Institute of Science and Technology (BIST)
Baldri I Reixac, 10–12, Barcelona 08028, Spain
E-mail: jramon@ibecbarcelona.eu

 The ORCID identification number(s) for the author(s) of this article can be found under <https://doi.org/10.1002/admt.202101696>.

© 2022 The Authors. Advanced Materials Technologies published by Wiley-VCH GmbH. This is an open access article under the terms of the Creative Commons Attribution-NonCommercial License, which permits use, distribution and reproduction in any medium, provided the original work is properly cited and is not used for commercial purposes.

DOI: 10.1002/admt.202101696

J. Comelles, E. Martínez
Department of Electronics and Biomedical Engineering
University of Barcelona (UB)
c/Martí i Franquès 1–11, Barcelona E08028, Spain
E. Martínez
Centro de Investigación Biomédica en Red (CIBER)
Av. Monforte de Lemos 3–5, Pabellón 11, Planta 0, Madrid E28029, Spain
A. García-Alamán, R. Gasa
Centro de Investigación Biomédica en Red de Diabetes y Enfermedades Metabólicas Asociadas (CIBERDEM)
Madrid 28029, Spain
A. García-Alamán, R. Gasa
Institut d'Investigacions Biomèdiques August Pi i Sunyer (IDIBAPS)
Barcelona 08036, Spain
J. Ramón-Azcón
Institució Catalana de Reserca i Estudis Avançats (ICREA)
Passeig de Lluís Companys, 23, Barcelona E08010, Spain

several functions: 1) suitable porous structure with mechanical stability, 2) excellent cytocompatibility to enhance cellular activity, 3) provide a physical barrier to protect embedded cells from cell to cell contact with the host's immune system.^[6] Furthermore, the semipermeable membrane should provide bidirectional transport of insulin, glucose, oxygen, and nutrients preventing central necrosis.^[7]

In recent years, encapsulated-based microspheres, or spheroids, are emerging as an optimal engineered tissue for graft implantation^[5,8] and *in vitro* drug testing.^[9,10] The 3D spheroids have the advantage of encapsulating large amounts of cells in a reduced volume, which helps deliver oxygen and nutrients to the core, simplified handling in a fluid suspension, and precise spatial and dosing control to fit *in vivo* applications.^[11] The standard techniques employed to fabricate hydrogel spheroids are currently based on microfluidics and electrostatic droplet generation. The first method is suitable for the rapid fabrication of spheroids by emulsion. However, the need for an oil phase containing surfactants, which negatively affects cell viability, is still its main limitation.^[7,12] On the other hand, electrostatic droplet formation avoids using the cytotoxic oil phase, but it requires biomaterials with high viscosity to maintain a spherical shape that is challenging to handle.^[13] Additionally, both methods are laborious, require considerable skill, and in addition, it is difficult to obtain uniformly sized spheroids. Therefore, there is an urgent need for more efficient and cost-effective strategies to produce cell-laden spheroids with high cell viability, controlling the diameter sizes and maintaining the spherical shape structure.

These technologies have widely used alginate hydrogel for appealing physical properties, such as lack of biodegradability, robustness, and economic cost.^[14] The alginate spheres are formed by combining the alginate solution with ionic cross-linking agents, such as divalent cations (i.e., Ca^{2+}). However, ionically cross-linked alginate hydrogels present limited long-term stability in physiological conditions, because they can be dissolved into the surrounding media due to the release of the divalent ions caused by the exchange reactions with monovalent cations.^[15] In addition, the calcium ions released from the gel may promote hemostasis, while the gel serves as a matrix for the aggregation of platelets and erythrocytes.^[16] Moreover, alginate revealed low biocompatible properties and limited control of mechanical properties.^[17] In this regard, collagen, the main supportive protein in the ECM, is getting recognized as an optimal biomaterial for cell-laden bioink. In the pancreas, collagens I and IV are abundant and widely expressed in mature human islets of Langerhans, where they support cell attachment and cohesiveness while also stimulating cell surface receptors to influence pancreatic cell proliferation and function.^[18] However, the self-assembled fibrillar structure is challenging to handle and is mechanically weak for direct use. A way to improve its mechanical stability is the further crosslink by a chemical agent such as glutaraldehyde,^[19] genipin,^[20] methacrylate,^[21] and by enzymatic crosslinker such as transglutaminase.^[22] Although these methods can improve some of the collagen's physical properties, their plethora of disadvantages range from cytotoxicity to expensive cost and excessive crosslinking time. Therefore, the formation of β -cell spheroids encapsulated in a non-cytotoxic collagen-based bioink is still needed.

To overcome the challenges in developing nontoxic biomimetic spheroids in an automatic way, we developed a high-throughput methodology using 3D bioprinter to encapsulate β -cells in a collagen bioink crosslinked with tannic acid (TA). This study aims to develop a new engineering strategy for the fabrication of an ECM-like environment that more closely mimics native islet conditions promoting cell-matrix interactions. We used collagen type I as a biocompatible encapsulation material that provides a physiological environment and mechanical support for the β -cell insulin production. In this study, rat insulinoma INS1E cells were encapsulated into 3D collagen-based microcapsules to investigate the substrate architecture's effect on cellular spatial organization, survival, and function. After spheroid fabrication, we examined cell viability and metabolic activity on days 1, 10, and 30. The results show that collagen crosslinked with TA scaffolds maintained cell viability for up to 30 days indicating preserved nutrient and oxygen diffusion. We also show that collagen fibrils treated with TA enhanced cell retention inside the spheroid compared to the pure collagen spheroids. In addition, INS1E spheroids improved glucose-induced secretion relative to cells maintained in 2D cultures. In summary, these results demonstrate that the high-throughput approach facilitates the fabrication of a cell encapsulation system that ensures good survival and functionality of insulin-producing β -cells. This strategy can help improve clinical outcomes of β -cell transplantation strategies for diabetes treatment.

2. Results and Discussion

2.1. Collagen-Based Hydrogel Characterization

TA is a specific class of hydrolyzable tannins containing a pentagalloylglucose core in which all hydroxyl functional groups are esterified by an additional gallic acid molecule (Figure 1a). The TA molecule interacts hydrophobically with collagen type I, forming hydrogen bonds with amino acid residues (Gly, Met, Glu, Ser, Arg, and Pro) in the collagen chain (Figure 1b).^[23] Additionally, TA possesses pleiotropic effects, such as antioxidant, anti-inflammatory, anti-bacterial, and anticancer properties.^[24]

We fabricated cylindrical collagen hydrogels without cells to evaluate the TA effects on the scaffolds. These scaffolds were generated at 37 °C to induce collagen fibril formation. One main property of TA crosslinking is the possibility to modulate the scaffold pore size by changing the concentration of TA used. Thus, collagen scaffolds were submerged into TA solution at 1% w/v (ColTA 1x) or 3% w/v (ColTA 3x) for 1 min (Figure 1c). Collagen samples were fragile and difficult to handle compared to ColTA hydrogels, which presented a more stable structure and were easy to handle and manipulate. At the ultrastructural level, in SEM images acquired after dehydration and critical point dry, we observed that TA generated significant changes in the collagen fibers within the hydrogels (Figure 1d). Specifically, TA crosslinking induced fusion of collagen fibrils, increasing their thickness and decreasing the pore size compared with non-crosslinked collagen hydrogels. Further, a uniform surface appeared when crosslinked for 10 min (Figure S1,

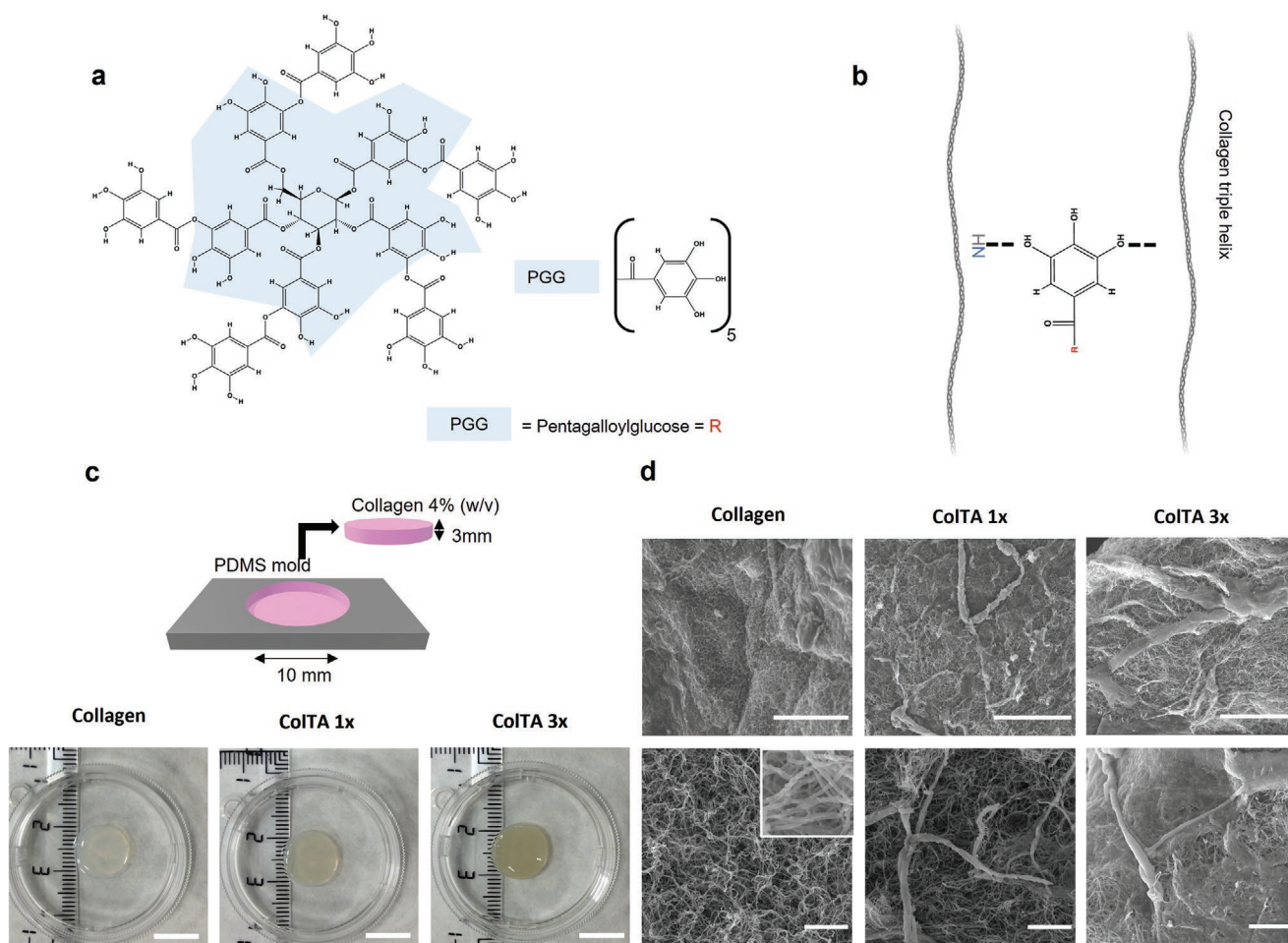


Figure 1. General overview of the collagen hydrogels crosslinked with two different weight fractions of TA 1 wt% (ColTA 1x), and 3 wt% (ColTA 3x) solutions used for this study. a) Chemical structure of TA. TA contains a pentagalloylglucose core in which all hydroxyl functional group are esterified by an additional gallic acid molecule. b) Hydrogen bond interactions between TA molecule and amino acid residues from the collagen peptide chain. c) Fabrication process scheme of the disc-shaped hydrogels used for the characterization tests. To generate cylinder-like scaffolds, a PDMS mold was filled with collagen prepolymer solution. Then, the mold was placed at 37 °C. Once the material crosslinks thermally, the scaffolds were submerged in TA solution for 1 min. Scale bar = 10 mm. d) Scanning electron microscope (SEM) images of the hydrogel porosity. First row scale bar = 50 μm . Second row scale bar = 5 μm .

Supporting Information). We determined the average pore size by analyzing SEM images. In the case of ColTA 1x, the average porosity was 0.09 μm , while in ColTA 3x was 0.07 μm , and in collagen, control was 0.12 μm (Figure 2a). By comparing different pore diameter ranges (Figure 2b), we noted an increment in the percentage of small pores related to the concentration of TA. The ability to decrease pore diameter by simply increasing TA concentration and/or crosslinking time is an interesting feature of our approach. While the porous mesh allows bidirectional transport of small molecules as insulin and glucose (0,0027 and 0,0015 μm , respectively),^[25] cells embedded in the hydrogel can be protected from cell-to-cell contact with human macrophages (21 μm)^[26] and T lymphocytes (7 μm).^[27] However, molecules as cytotoxic cytokines released by the host immune system, such as interleukin 1b (0,0024 μm),^[28] are still permeable and could contribute to the death of the transplanted β -cells. Current live-cell encapsulation technologies face a trade-off among several major considerations. Enhancement of one consideration may sacrifice the other. For example, a

thick membrane with good immune isolation and mechanical stability often leads to poor nutrient/oxygen supply. A more in-depth study is required to reach a good compromise between the preservation of β -cell functional features, i.e., insulin secretion and cytokine protection.

Next, we checked scaffold swelling properties. To measure the diffusion of the nutrients indirectly through the scaffolds, we analyzed the swelling ratio. Swelling is the water uptake capability of a hydrogel, an indirect measurement of pore interconnectivity.^[29] After only 24 h, the hydrogels reached an equilibrium, with a swelling ratio of 53.63 \pm 6.11% for collagen, 35.73 \pm 2.44% for ColTA 1x, and 30.81 \pm 1.94% for ColTA 3x (Figure 2c). Although this property was higher in collagen than in ColTA conditions, as expected, all the scaffolds presented permeability. These percentages of swelling indicate that the scaffold's structures were highly interconnected, as water could colonize all the structures. The reduction in swelling ratio of ColTA conditions could be due to the decrease in the number of hydrophilic groups in the presence of TA, which increased

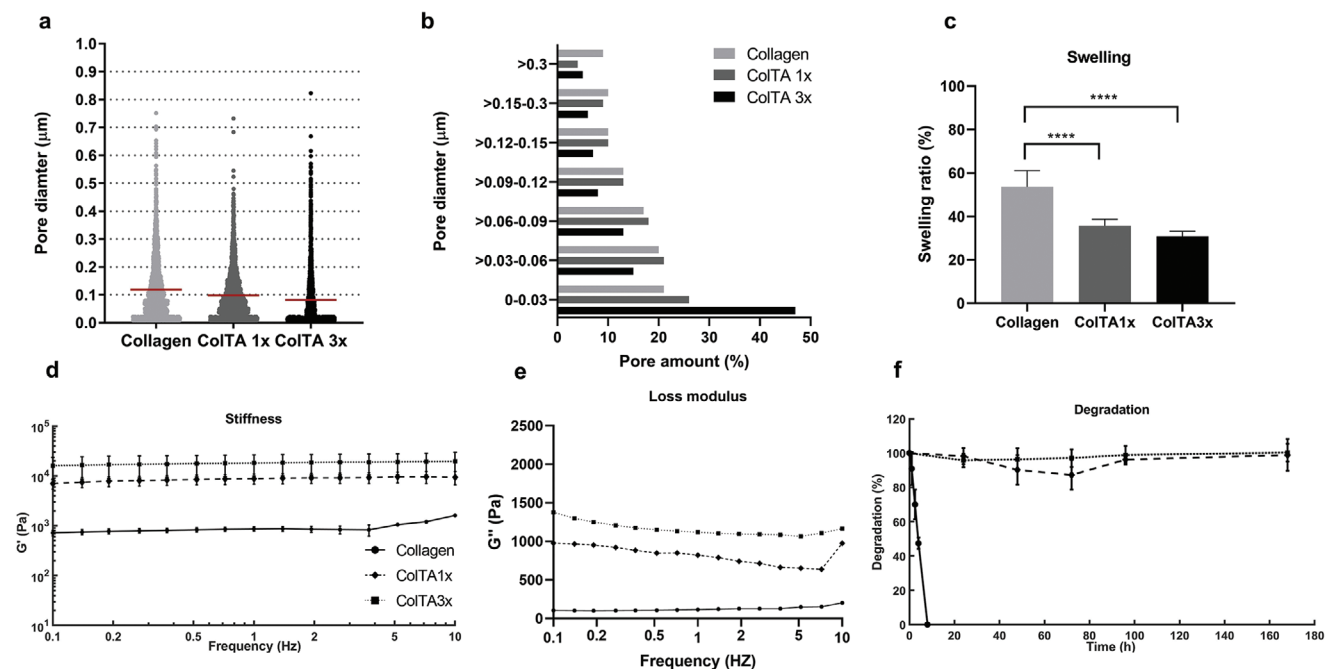


Figure 2. Mechanical characterization of the scaffold. a) Pore distribution using different concentrations of the TA crosslinking solution. b) Percentage of pores in different diameter ranges according to the concentration of the TA. Of note, the higher the concentration, the higher the percentage of pores between 0–0.03 μm of length. c) Swelling ratio. d) Rheological stiffness results. e) Rheological loss modulus results. f) Percentage of weight loss using the collagenase type I to examine the degradation of collagen-based scaffolds. Results are expressed as the mean \pm SEM from at least three independent experiments ($n = 9$). **** $p < 0.0001$.

the hydrophobicity of the hydrogels. Even so, the strong point of this approach was the capability of the scaffolds to be permeable, allowing the diffusion of oxygen and nutrients through the hydrogels. Moreover, in other approaches, the swelling ratio of pure collagen hydrogel was set as $\approx 50\%$,^[30] a value that fits with the scaffold swelling achieved.

Another feature that we studied was scaffold stiffness. The ECM supports cells and plays an important role in regulating cell behaviors such as cell spreading, migration, proliferation, and differentiation.^[31] It is composed mainly of collagen fibers which cells are in contact with and sense through mechanotransduction.^[32] Therefore, the final stiffness contribution mainly depends on collagen abundance and organization.^[33] As we wanted to mimic the ECM and the pancreatic islet environment, the collagen scaffolds stiffness was an essential property to analyze. Moreover, knowing that cells modulate their behavior in different substrate stiffness,^[34,35] maintaining a similar stiffness as soft tissues should help to the viability and the functionality of the embedded cells. Rheometer analysis was performed to measure the stiffness of the scaffolds. Rheology studies the relationship between force (stress) and deformation (strain) under a constant frequency.^[36] This dynamic analysis was performed by applying a viscoelastic strain in cycles repeatedly over time to yield elastic (storage) and viscous (loss) moduli. The storage modulus is related to elastic deformation of the material (G'), whereas the loss modulus represents the energy dissipated by internal structural rearrangements (G''). The results obtained confirmed the increase in stiffness after crosslinking hydrogels with TA as demonstrated by storage modulus (Figure 2d). The G' value in the collagen condition

was 0.9 kPa and increased to 8.6 to 15 kPa with TA solution 1x and 3x, respectively. The frequency-dependent measurements of our hydrogels from all formulations showed that the storage modulus (G') was always higher than the loss modulus, showing that the hydrogels were predominantly elastic (Figure 2e). The stiffness achieved correlates well with the proper stiffness defined for soft tissues which range from 0.1 to 100 kPa.^[32] In addition, our values are in good agreement with previously reported values for collagen and collagen crosslinked with TA hydrogels which range from 0.61 to 67.13 kPa.^[37] Moreover, the increment in stiffness in ColTA conditions was in accordance with the increase of collagen fiber fusion and the diminution of pore size shown previously in Figure 2a,b.

To assess whether the increased stiffness of hydrogels crosslinked with TA confers higher resistance to enzymatic degradation, we incubated the collagen, ColTA 1x, and ColTA 3x hydrogels with Collagenase type-I (see Experimental Section). Collagen hydrogels treated with TA showed higher resistance to collagenase degradation compared with pure collagen. Figure 2f shows the percentage of weight loss using collagenase type I to examine the degradation of the collagen hydrogels in different crosslinking conditions. Non-crosslinked scaffolds underwent a complete degradation in 8 h, while ColTA hydrogels remained stable against collagenase and did not show any degree of degradation over the 7 days of the experiment. Thereby, the TA molecule is bound strongly to collagen and stabilized collagen. One explanation is that the hydrophobic interaction of TA with the amino acid residues of collagen cause that collagenases fail to recognize their cleavage site in collagen structure.^[21,38] We can conclude that our scaffolds satisfy all the mechanical

and physical needs of the β cells. The in vivo degradation of collagen-based spheroids was evaluated by spheroid transplantation into immunodeficient NOD Scid Gamma (NSG) mice. ColTA 1x and 3x spheroids were implanted on the omentum surface, considered a favorable environment for cell survival and function,^[39] and fixed by folding the tissue. After 15 and 30 days, the animals were sacrificed to assess the integrity of the scaffold. As shown in Figure S2 (Supporting Information), the crosslinked spheroids persisted at days 15 and 30, allowing the spheroids constructs to be readily identified and retrieved. Overall, these results show a well-defined and reproducible method to afford non-degradable and microporous cell-supportive scaffolds.

2.2. Tunable Stiffness of Collagen-Based Hydrogels

Numerous studies have described the effects of matrix stiffening on cell behavior using 2D synthetic surfaces; however, less is known about the effects of matrix stiffening on cells embedded in 3D in vivo-like matrices. A primary limitation in investigating the effects of matrix stiffness in 3D is the lack of materials that can be tuned to control stiffness independently of matrix density. Recent efforts to modulate 3D matrix stiffness have included modifying matrix density of natural proteins^[40–42] and alginate,^[43] using synthetic polymers with tunable crosslinking densities such as poly(ethylene) glycol (PEG) to create hydrogel scaffolds.^[44,45] Although these modifications are capable of generating 3D scaffolds with tunable mechanical properties, they also increase the density of the matrix, causing changes in the porosity and the number of cell binding sites. Here we were interested in developing mechanically tunable collagen-based microspheres. To study the stiffness gradient across the spheroid radius due to the TA diffusion, we designed an experimental setup approximation. This approximation consisted of a rectangular prism inscribed in a sphere with a radius of 5 mm (Figure 3a). We used a PDMS mold containing an empty pool at one end to fabricate the rectangular hydrogel. Then, we filled the empty pool with TA 1x solution for 1 min. Finally, we measured the local stiffness along the rectangular hydrogel length by AFM (Figure 3b). The end of the rectangular hydrogel in contact with the TA pool exhibited high stiffness values which were declining along with the hydrogel, generating a stiffness gradient (Figure 3c). Thereby, we were able to tune the stiffness of the collagen hydrogel in a range between 100 to 2 kPa. Additionally, confocal reflection images revealed a higher presence of a brighter structure at the end of the rectangular stripe in contact with TA solution than the other end (Figure 3d). ColTA hydrogels exhibited thicker fiber bundles than non-treated collagen in a time-dependent manner. Overall, we have described a method to modulate the 3D stiffness of fibrillar collagen scaffolds, minimally altering the inherent fiber structure without the addition of synthetic materials.

2.3. Collagen-Based Hydrogel can be Used as A Suitable Bioink for Spheroid Fabrication Using 3D Bioprinter Technology

To generate a functional 3D structure to support β cells, we encapsulated INS1E cells into the collagen hydrogel spheroids

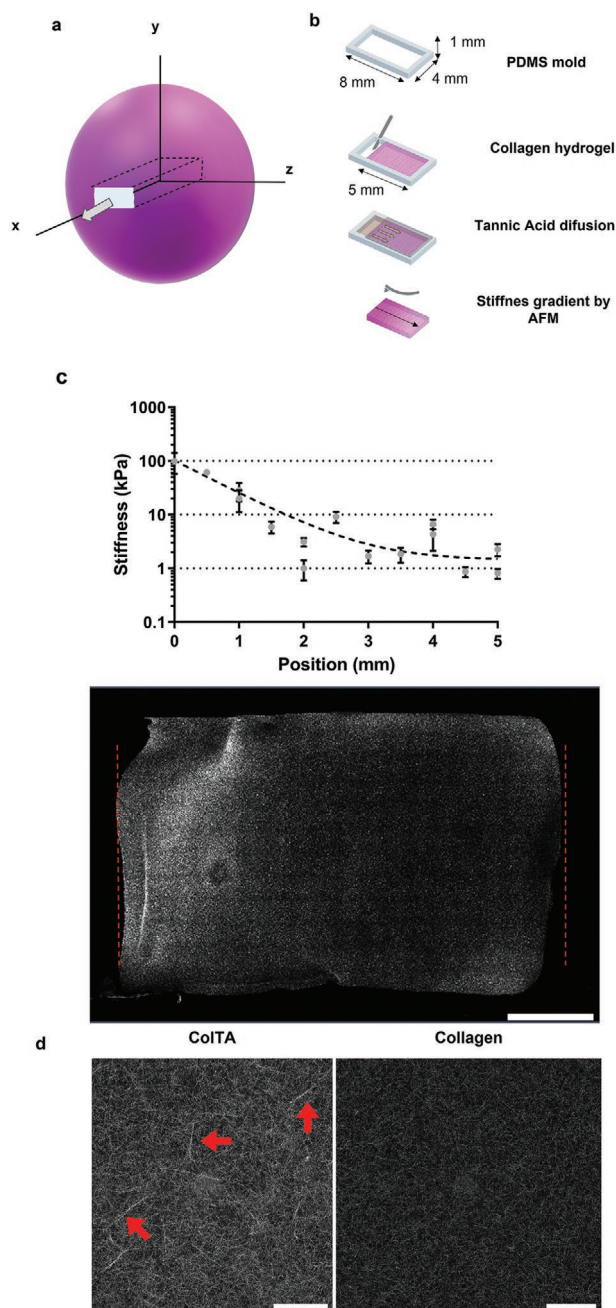


Figure 3. Characterization of tannic acid diffusion across the collagen-based stripe in a gradient mode. a) Rectangular model approximation based on a rectangular prism inscribed in a radius of 5 mm, to study tannic acid diffusion along the x-axis. b) The microrheology of the hydrogels was probed with an Atomic Force Microscope (AFM). Note that stiffness decreases along the rectangular stripe confirming that tannic acid diffuses while crosslinking the hydrogel. c) Representative reflection microscopy image of collagen-based rectangular stripe used for the AFM analysis. Scale bar = 1000 μ m. Results are expressed as the mean and SD ($n = 3$). d) Reflection microscopy images of collagen and ColTA 1x hydrogels crosslinked for 1 min period. Note that thicker fiber bundles appear in collagen treated with TA (red arrows). Scale bar = 50 μ m.

using the 3D bioprinter (see Experimental Section). The fabricating process of cell-laden spheroids is shown in Figure 4a.

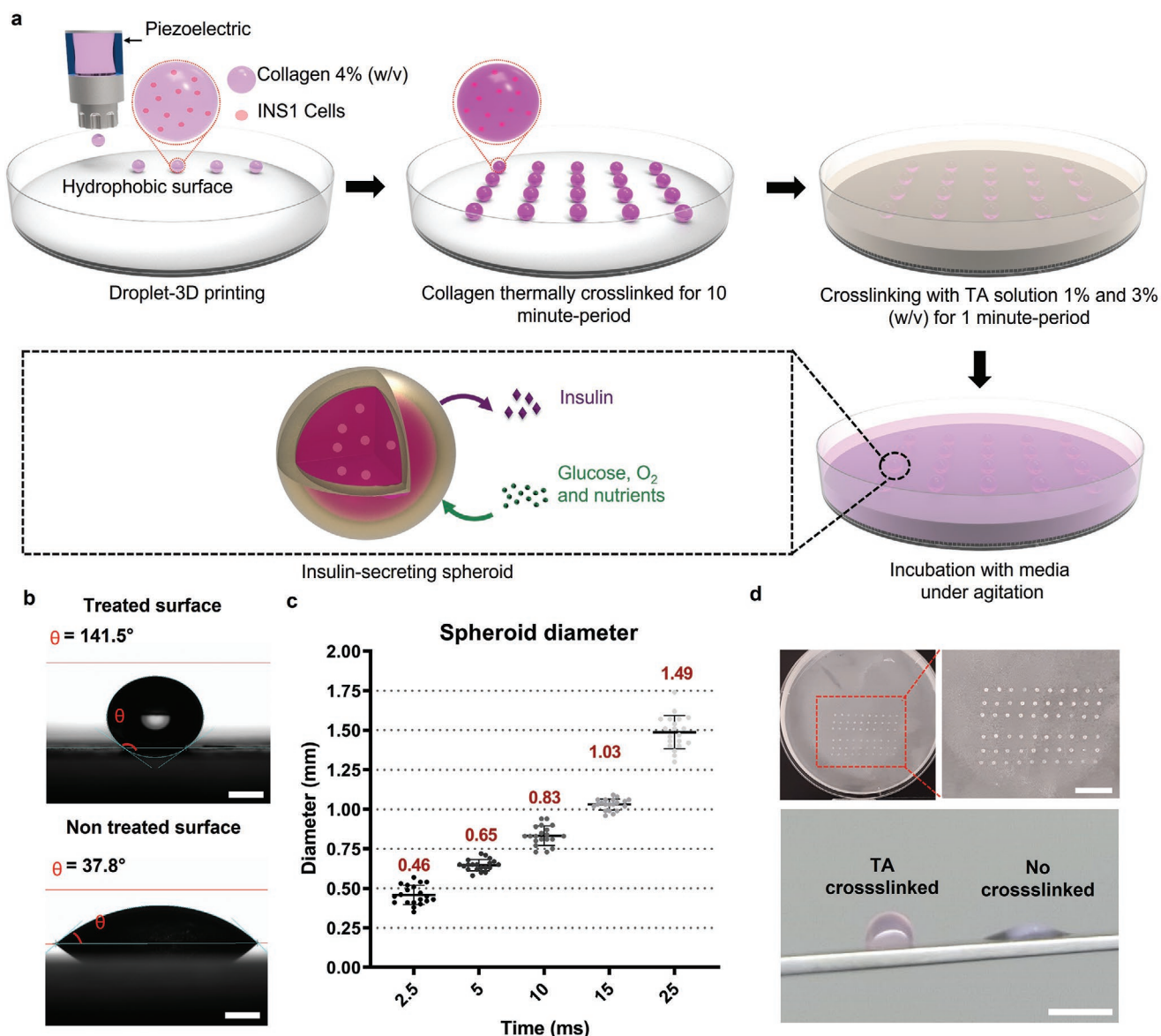


Figure 4. Cell-laden spheroids generated by the novel 3D bioprinter technique. a) Schematic depiction of INS-1E-laden spheroids fabrication crosslinked using different concentrations of TA solution. b) Contact angle differences between a hydrophilic and hydrophobic substrate. Optical images of the cell-laden spheroids generated by the inkjet/valve printhead of the 3D bioprinter. c) Spheroid diameter range generated using the inkjet/valve printhead. Of note, a shorter obturation time of the valve translates into a lower volume of hydrogel deposited onto the superhydrophobic surface, thereby reducing the diameter of the spheroids. Results are expressed as the mean and SD ($n = 20$). d) Images of a square array of 60 spheroids of 0.83 mm diameter, fabricated using the 3D bioprinter. Scale bar = 10 mm. Collagen crosslinked with TA spheroid compared to collagen control spheroid. Scale bar = 10 mm.

Briefly, the inkjet/valve printhead was loaded with the cell-laden collagen bioink. The hydrophobic petri dish was placed on the system working stage. A square array of 60 spheroids was fabricated with a cell density of 7×10^6 cells mL⁻¹ (Figure 4d). Spheroids were thermally crosslinked at 37 °C for 10 min. As before, 1% and 3% (wt/v) TA concentrations were used to examine their effects on cellular activities.

First, to characterize the hydrophobicity of the plate, we measured the contact angle of the spheroid with the surface. As shown in Figure 4b, the hydrophobic surface maintained the spherical shape of the hydrogel drop, showing a contact angle

of 141.5°. In contrast, the non-treated plate allowed the droplets to spread out with a smaller contact angle of 37.8°. In conclusion, the superhydrophobicity of the pre-treated plates allowed the spherical shape of collagen hydrogel drop.

On the other hand, a common drawback in spheroid cultures is the inadequate supply of nutrients and oxygen to the core of the spheroid. Previous studies demonstrated that increasing spheroid diameter decreased glucose and oxygen concentration inside the spheroid^[46–48] and resulted in the inefficient removal of discarded metabolites.^[7] For this reason, we aimed to fabricate cell-laden spheroids in a wide range of sizes using the 3D

bioprinter. For in vivo long-term applications, it is crucial to decide on an appropriate spheroid diameter with suitable diffusivity properties that fit with the implementation site.

We took advantage of the inkjet/valve printhead to produce a range of different diameter sizes, which incorporates a piezoelectric valve. The operator can control the opening and closing time of the valve. A shorter obturation time translates into a lower volume of hydrogel deposited onto the superhydrophobic surface and vice versa. The bioprinter system was then applied to produce controlled droplet arrays that can fabricate 100 spheroids/min with a well-controlled diameter size. We fabricated spheres of up to 5 different diameters using different hydrogel volumes. We successfully produced spheroids with a diameter ranging from 0.46 ± 0.06 to 14.9 ± 0.03 mm by changing the valve-opening duration from 2.5 to 25 ms, respectively (Figure 4c). Overall, we produced spheroids with tunable sizes by using the 3D bioprinter technique.

One more exciting aspect is that after being crosslinked with TA, spheroids increased the stability of the entire structure, allowing us to obtain perfect microspheres that tolerate intense mechanical manipulation without losing their morphology (Figure 4d).

2.4. Collagen-Based Hydrogels Crosslinked with TA Maintain Cell Viability and Promote Cell Retention Inside the Spheroids

Next, we sought to establish cell viability during long-term in vitro culture of the cell-laden spheroids. Cell viability in spheroids of 0.83 mm diameter was assessed at days 1, 10, 30 by Live/dead assay. A qualitative examination of the fluorescence images revealed homogeneous cell distribution within the spheroids (Figure 5a). On day 1 after encapsulation, spheroids presented lower viability as compared to days 10 and 30. The shear stress present at the nozzle during the fabrication process is the main cause of cell damage and loss.^[49] Remarkably, we found similar viability in collagen and ColTA spheroids at all times studied (Figure 5b). These data indicate that 0.83 mm diameter spheroids represent a good compromise between cell viability, ease of handling, and visibility and hence were used in subsequent experiments.

Changes in metabolic activity can be easily quantified with the Alamar blue assay. While metabolic activity was similar in collagen and ColTA spheroids at day 1, it was significantly lower in ColTA spheroids compared to collagen spheroids at day 10 (Figure 5c). Surprisingly, on day 30, results showed increased metabolic activity of ColTA 1x spheroids compared to collagen and ColTA 3x spheroids. These results demonstrated that TA did not affect cell viability inside the spheroids for up to 30 days in culture.

Another exciting feature that we wanted to study was the ability of the collagen crosslinked with TA hydrogels to retain the cells inside the microcapsules. The ability of the cells to migrate or proliferate outside the biomaterial is a critical point in the tissue replacement therapies field regarding the biosafety of the patient. Biomaterials must keep cells inside the structures to prevent their spread in the body, eliminating the possibility of teratoma formation.^[48,49] It has previously been reported that density and spatial alignment of the collagen

architecture can guide cell migration and leaking. To confirm that, the whole cell-laden collagen scaffolds were monitored to check cell release/leaking from the spheroids over time. In the collagen control condition, single INS1E cells were detected outside the spheroids on days 1, 10, and 30. In contrast, free cells were rarely found outside the ColTA 1x and ColTA 3x spheroids (Figure 5d), suggesting a marked increase in cell retention after the TA treatment. Indeed, collagen spheroids at day 1 released 359 ± 117 cells compared to 4 ± 1 cell in the ColTA 1x and 3 ± 2 in ColTA 3x, reaching 92,05% less cell leak between collagen and ColTA 1x. Over time, collagen spheroids decreased the number of leaked cells from 172 ± 70 cells at day 10, to 70 ± 16 cells at day 30, while the ColTA spheroids maintained a cell scaping of 3 ± 1 cells in ColTA 1x and 2 ± 1 cell in ColTA 3x for the 30 days. These results show that the crosslinked collagen fibrils treated with TA promoted cell retention inside the spheroid compared to the pure collagen spheroids. The cell retention effects of this highly compacted collagen network correlate with the physical changes in stiffness and porosity described in biomaterial characterization (Figure 2a–d).

2.5. ColTA 1x Spheroids Secrete Insulin and Can be A Suitable Model for the Study of the β -Cell Function

We performed confocal image analysis of insulin and DAPI expression in INS1E-containing spheroids. As expected, all cells in spheroids expressed insulin, and, in agreement with images in Figure 6a, cells were homogeneously distributed in all conditions at day 10 after encapsulation. The different z-stacks of spheroids per condition showed uniform distribution of insulin staining all over the spheroids (Figure 6a). Interestingly, in both collagen and ColTA hydrogels, cells were able to proliferate, as we qualitatively analyzed by immunodetection of the ki67 proliferation marker (Figure S3, Supporting Information).

It has been described that cell-matrix interactions improve β -cell survival and insulin secretion in 3D culture.^[50] Lastly, to determine whether encapsulated INS1E cells into 3D hydrogel exhibited increased β -cell function, we tested the insulin secretory response to glucose of the cell-laden spheroids compared to 2D monolayer culture. A GSIS assay, which defines the ability of β -cells to secrete a suitable amount of insulin in response to extracellular glucose stimuli, was performed in all conditions to check islet functionality. As shown in Figure 6b, collagen and ColTA 1x spheroids improved the insulin secretion stimulation index in response to glucose compared to 2D monolayer culture. Moreover, both conditions presented similar insulin secretion values. Indeed, on day 7, INS1E cells seeded in a 24 well-plate presented a 2.62 ± 0.4 fold-increase of insulin secretion when cells were challenged with 16.7×10^{-3} M compared to cells incubated with 2.8×10^{-3} M glucose. Collagen spheroids showed a 3.77 ± 1.2 fold-increase. Interestingly, we reached a fold increase of 3.95 ± 1.3 of insulin secretion when ColTA 1x spheroids were challenged with 16.7×10^{-3} M glucose. By contrast, insulin secretion by ColTA 3x spheroids was nearly undetectable, revealing that this TA concentration hinders proper insulin output. This observation might be explained by the difficulty for insulin to break through the small-sized pores from the fused collagen fibers. Therefore, our study validates

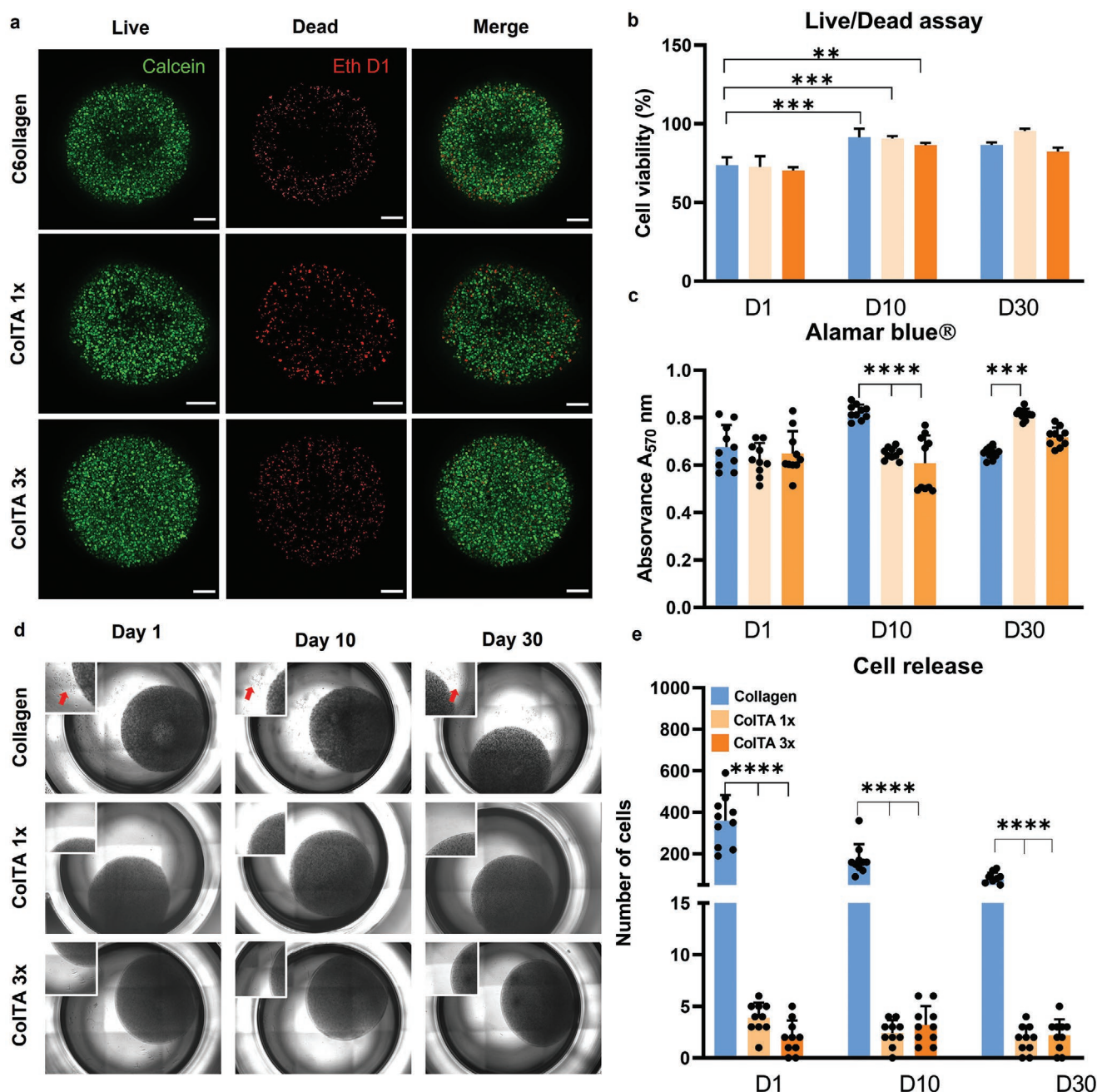


Figure 5. In vitro cell viability and analysis of cell release from cell-laden spheroids a) Representative fluorescent images of INS1E Live/Dead at day 10 after encapsulation. Live cells are marked with Calcein AM in green, and dead cells are marked with EthD-1 in red. Scale bar = 500 μ m b) Cell viability assay of INS1E cells at day 1, 10, and 30 encapsulated into the spheroids. c) Alamar blue test of collagen-based spheroids after day 1, 10, 30 of encapsulation. Almar blue assay was detected at 570 nm. d) Optical images of cell release test after 1, 10, and 30 days of culture. e) Number of cells that were able to escape from the spheroids at day 1, 10, and 30 of culture. Results are expressed as the mean and SD ($n = 10$). $***p < 0.01$ $****p < 0.001$ $*****p < 0.0001$.

that a 3D mesh structure mimicking the in vivo ECM ensures an optimal insulin response of embedded β -cells provided a TA concentration $< 3x$.

3. Conclusions

The field of tissue engineering has experienced remarkable progress with the incorporation of novel technologies as 3D

bioprinting. This technology opened new opportunities to generate more replicable, customized, and cost-optimized engineered tissues. Otherwise, collagen-based materials have been recognized as promising to accomplish an ideal mimetic bioink for cell encapsulation with high cell-activating properties.

However, despite the wide range of outstanding biological properties, the use of collagen has been limited due to its characteristic low mechanical strength.

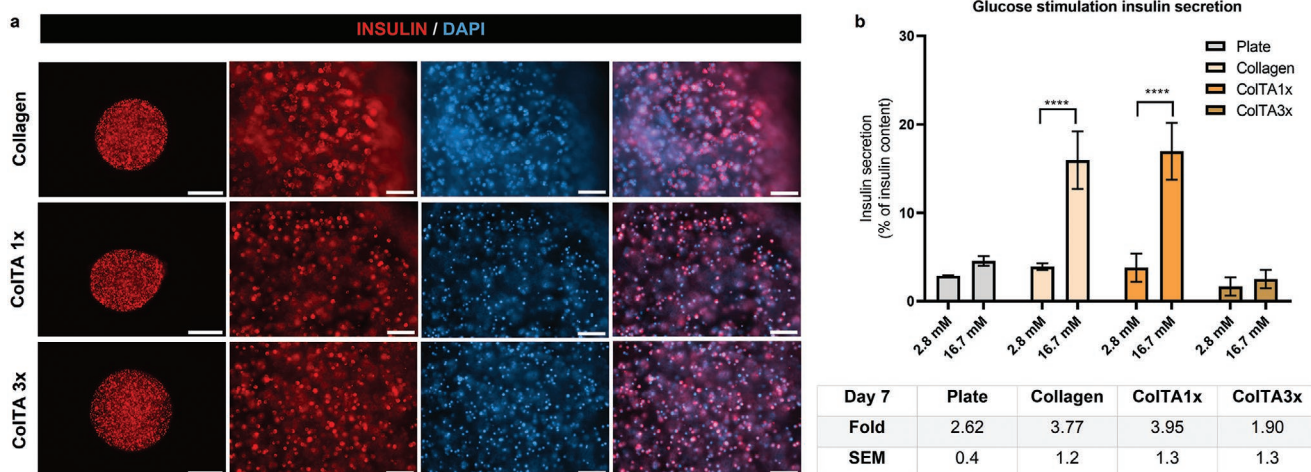


Figure 6. Collagen crosslinked with TA enables insulin secretion. a) Representative images of INS1E cells encapsulated in the spheroids at day 10 insulin (red) and nuclei (DAPI). First column scale bar = 500 μm and others 100 μm . b) Glucose stimulation insulin secretion (GSIS) assay at day 8 in pristine collagen and ColTA spheroids. For the GSIS assays, cells were incubated for one hour at 2.8×10^{-3} M glucose, followed by 16.7×10^{-3} M glucose. Results are expressed as the percentage of insulin secreted related to the total insulin content of the corresponding sample \pm SEM from three independent experiments, each one including at least 3 different replicates per condition. **** $p < 0.001$.

In this study, we described a novel methodology to 3D-bioprint collagen solution in the form of cell-laden spheroids. The spheroids were post-treated with TA crosslinking solution, which provided structural consistency and protected the embedded cells from the degradation of collagenase I.

This hydrogel possessed a well-organized microstructure with adjustable mechanical stiffness and porosity. Moreover, viability tests demonstrated that the ColTA spheroid is an excellent encapsulating material that permits good gas and nutrient exchange. Also, we demonstrated that the optimal concentration of TA to ensure glucose-induced insulin secretion was 1 wt% (ColTA 1x condition).

Significantly, the reduced spheroid volume and the increment of surface-area-to-volume ratio could improve the diffusion distance compared to large volumes leading to a significant decrease in time response to blood glucose changes. Finally, this protocol allows the encapsulation of a large number of cells in a short period (less than 1 min), preventing them from hypoxic stress that can cause cell function loss. Furthermore, in vivo studies showed that transplanted structures did not present any sign of degradation, demonstrating its non-biodegradability property and highlighting the feasibility of using this strategy as a potential therapy for T1D.

In summary, the present study provides a foundation toolset to generate cell-laden spheroids using a 3D bioprinter approach, which can be helpful for future advanced functional studies. (e.g., with more clinically relevant cells such as iPSC-derived β cells or dissociated primary islets). This technology can be applied to encapsulate a wide range of transplantable cell types. Also, by adding components of the extracellular matrix to the collagen-based hydrogel, it could be possible to obtain a more cell-laden matrix similar to the native environment found in vivo.

4. Experimental Section

Preparation of Collagen-Based Solutions: Type I collagen from rat tail (Corning) at 8.43 mg mL^{-1} was used for the standard working solution. Collagen was dissolved with 10x PBS (Sigma) at the ratio of 1:10 and neutralized with 1 M NaOH (PanReac-AppliChem) to achieve a pH of 7.5. The resulting hydrogel solution was dissolved with RPMI 1640 medium (Gibco) to reach the final concentration of 4 mg mL^{-1} .

Scanning Electron Microscopy: Collagen hydrogel solution was poured in a cylindrical PDMS (DOW Corning, SYLGARD 184) mold of 10 mm diameter and 3 mm height (Figure 1c). Collagen hydrogel was thermally crosslinked after 10 min at 37°C . Next, collagen hydrogels were detached from the mold and submerged in a TA solution (Sigma) at 1% w/v (TA 1x) and 3% w/v (TA 3x) in PBS 1x, for 1 min period. Finally, the collagen-based hydrogel crosslinked with TA 1x (ColTA 1x) and TA 3x (ColTA 3x) were washed twice with 1x PBS. After that, dehydration was carried out by sequential immersion in graded ethanol solutions in Milli-Q water: 30%, 50%, 70%, 80%, 90%, and 96% v/v for 10 min each and twice for 100% ethanol. Then, samples were placed in a critical point dryer (K850, Quorum Technologies, UK), sealed, and cooled. Ethanol was replaced entirely by liquid CO_2 and by slowly heating. After critical point drying, hydrogels were covered with an ultra-thin coating gold and imaged by ultrahigh-resolution scanning electron microscopy (SEM). Pore diameters were quantified with ImageJ version 1.52b software (National Institutes of Health).

Swelling: Swelling is the water uptake ratio by a scaffold. Hydrogels were fabricated as explained previously and were weighed after fabrication to measure this. Next, cryogels were submerged into MilliQ water for 24 h when they reached equilibrium and weighed again. The swelling ratio was calculated as follows:

$$\text{Swelling ratio} = \frac{W_e - W_f}{W_f} \times 100 \quad (1)$$

Where W_e is the weight in equilibrium and W_f is the weight after fabrication. Three hydrogels per condition were measured in this assay.

Stiffness Characterization: Mechanical properties of hydrogels were assessed using a parallel plate rheometer (Discovery HR-2 rheometer, TA instruments, Inc., UK). Hydrogels were fabricated in a cylindrical shape (1 mm thick, 8 mm diameter), and bulk modulus (G') and viscous modulus (G'') measurements were recorded at a frequency range of 1–10 Hz at room temperature using 8 mm aluminum plate geometry. The gap

was adjusted starting from the original sample height and compressing the sample to reach a regular force of 0.3 N. Rheological measurements were made on hydrogels after 24 h post crosslinking.

Degradation: Cylinder-shaped hydrogels, 8 mm in diameter, were fabricated as described above for the degradation analysis. Hydrogels were submerged in 1x PBS solution and left swelling for 1 day. A total of 2 mL of 0.25 U mL⁻¹ Type-I-Collagenase from *Clostridium histolyticum* (Sigma) dissolved in 5 × 10⁻³ M CaCl₂ with TBS1x was added to the hydrogels. Then, hydrogels were weighed after 1, 2, 4, 24, 48 h, 72 h, 96 h, and 7 days. The percent hydrogel remaining (%Wr) was determined by the following equation:

$$\% Wr = \frac{W_t}{W_i} \cdot 100 \quad (2)$$

Where W_t and W_i are the weights of hydrogels before and after the collagenase incubation.

TA Diffusion: The collagen type I hydrogel solution was prepared using a PDMS mold of 8 × 4 × 1 mm (Figure 3b). A volume of 50 μL of the hydrogel solution at 4 mg mL⁻¹ was poured and allowed to crosslink thermally at 37 °C for 10 min. The rectangular hydrogel was cut to create a pool. The pool was filled with a TA 1x solution for 1 min, performing a crosslinking gradient across the hydrogel. Then the hydrogel was removed from the mold and rinsed with PBS. The hydrogels micro-rheology was probed with an Atomic Force Microscope (AFM) NanoWizard 4 Bioscience AFM (JPK Instruments) mounted on the stage of an inverted optical microscope (Nikon Eclipse Ti-U). Silicon-Nitride V-shaped cantilevers with a constant force of 0.08 N m⁻¹, resonance frequency of 17 kHz, and cantilever length of 200 μm (Nanoworld innovative technologies, PNP-TR-50) were used to analyze samples. The force-distance curves obtained were fitted to obtain the elastic modulus, using the Hertz model for a pyramidal tip (JPK data analysis software).

Reflection Microscopy Images: Fiber differences between collagen and ColTA hydrogels were visualized using 35 mm glass-bottom dishes (MatTek). A volume of 50 μL of cold collagen (4 mg mL⁻¹) was deposited over the glass bottom. Next, dishes were centrifuged at 2000 rpm for 3 min and incubated at 37 °C for 20 min. The collagen hydrogel was submerged in 500 μL of TA 1x solution for 1 s, 1 min, and 10 min. The resulting hydrogels were imaged using confocal reflection microscopy inverted Zeiss LSM-780, with a 32x water immersion objective with a numerical aperture of 0.85.

Superhydrophobic Surface: Ultra-Ever Dry (SE 7.6.110) solutions based on two-part coating compounds (bottom and top) were used to create hydrophobic surfaces. The surface activation of standard Petri dishes (ThermoFisher) was achieved following the manufactured instructions. The bottom coat solution was briefly shaken in a fume hood and applied over the Petri dish to obtain a 1.0 mil film. After 20 min, the topcoat was applied until a translucent white surface was seen. The plates became hydrophobic after 2 h.

Spheroid Fabrication Using 3D Bioprinter: The process of β-cell spheroid formation is illustrated in Figure 4a. This work used a fixed concentration of collagen type-I (4 mg mL⁻¹) and INSIE cells as a bio-ink. Collagen was mixed with the cell density of 7 × 10⁶ cells/ mL. A bioprinter platform (3DDiscovery, regenHU Ltd) with inkjet/valve printhead (Microvalve CF300, MVJ-D0.1S0.06) was used to fabricate the spheroids. The hydrophobic petri dish was placed on the system working stage, and the syringe was filled with the cell-laden hydrogel.

Square array patterns of 50 points were designed using the BioCAD v1.0 software (regenHU Ltd) and launched to the bioprinter platform (Figure 4a). The optimal printability was achieved with a nozzle diameter of 0.15 mm, pneumatic pressure of 0.2 bar, and printhead temperature of 6 °C. To obtain collagen spheres with different diameters: 1.49, 1.03, 0.83, 0.65, and 0.46 mm, a valve-opening duration of 25, 15, 10, 5, and 2.5 ms was applied, respectively.

It was decided to work with a diameter size of 0.83 μm, equivalent to a valve-opening duration of 10 ms. After printing, the cell-laden collagen spheroids were thermally crosslinked at 37 °C for 10 min. The collagen spheroids without crosslinking process were used as a control, and the spheroids were crosslinked with two different concentrations, 1x and 3x,

for 1 min. After several washes with PBS 1x, the spheroids were placed in a 24 non-treated MW plate (Costar) and cultured in 3D suspension in constant stirring, with low growth medium based on RPMI 1640 medium (Gibco) supplemented with glucose (5.5 × 10⁻³ M), 5% fetal bovine serum (FBS) (v/v), 10 × 10⁻³ M HEPES, 2 × 10⁻³ M L-glutamine, 1 × 10⁻³ M sodium-pyruvate, 0.05 × 10⁻³ M 2-mercaptoethanol and 1% penicillin/streptomycin (v/v).

Cell Culture: Rat pancreatic β-cell line INSIE cells were cultured in high growth medium based on RPMI-1640 (Sigma) with 11.1 × 10⁻³ M glucose, supplemented with 10% fetal bovine serum (FBS) (v/v) (ThermoFisher), 10 × 10⁻³ M HEPES (Gibco), 2 × 10⁻³ M L-glutamine (Gibco), 1 × 10⁻³ M sodium-pyruvate (Gibco), 0.05 × 10⁻³ M 2-mercaptoethanol (ThermoFisher), and 1% penicillin/ streptomycin (v/v) (ThermoFisher). When cells reached confluency, cells were trypsinized with 0.25 Trypsin/0.1% EDTA and plated in a new flask at 1:4 density. Cells were maintained in an incubator at 37 °C and 5% CO₂.

In Vivo Biodegradability Study: NSG mice were used to assess the in vivo evaluation of collagen-based spheroid biodegradability. Acellular collagen spheroids crosslinked with TA were fabricated using the 3D bioprinter. Subsequently, the spheroids were crosslinked with TA 1x and 3x for 1 min. For each condition, 3 spheroids were transplanted per mouse. The selected location was the bursa omentalis. The in vivo transplant was evaluated after 15 and 30 days. The local ethical committee for animal experimentation of the University of Barcelona approved all animal experiments and procedures. 345/18-P3 (CEA UB), 10239P3 (Generalitat Catalunya).

Live/Dead: Viability assays were performed with the Live/Dead assay kit (ThermoFischer) according to manufacturer instructions. The assays were performed on days 1, 10, and 30 of culture after cell encapsulation. Briefly, the spheroids were washed 5 min with PBS three times to replace the culture medium and incubated with the working solution (12 × 10⁻⁶ M EthD-1, 3 × 10⁻⁶ M Calcein AM, and 12 × 10⁻⁶ M Hoechst) for 25 min at 37 °C in agitation. Then spheroids were washed three times with PBS. Finally, confocal images were taken using a Zeiss LSM 800 confocal microscope. The quantification of the Live/Dead assay ratio was calculated as follows:

$$\text{Live ratio} = \frac{\# \text{ Live cells}}{\# (\text{Live cells} + \text{Dead cells})} \times 100 \quad (3)$$

Alamar Blue: AlamarBlue (ThermoFisher) was performed according to manufacturer specifications. Shortly, each spheroid was placed in a 96-well plate throughout the experiment ($n = 10$). The medium was removed from the well plate and replaced by 11.1 × 10⁻³ M of glucose medium RPMI-1640 with a 1:10 dilution of AlamarBlue. After 3 h incubation, 100 μL of each condition were placed in a well of 96 well-plate and read in a Power wave X microplate spectrophotometer at 570 nm.

Releasing Cell Test: The releasing cell assay was performed to evaluate the number of cells able to escape from the biomaterial. Briefly, single spheroids were placed in 96 well-plate and incubated for 1, 10, and 30 days. The escaped cells were counted both in medium and cells attached to the bottom of the plate. For the cells attached, 50 μL of trypsin-EDTA (0.025%) was added to the well and incubated for 10 min. The pellet was resuspended in 10 μL and mixed with 10 μL of trypan blue 0.4% (ratio 1:1) (15250061, Thermo Fischer) and counted using an automated cell counter Countess (Fisher scientific).

Immunostaining: For confocal analysis, stained cell-laden spheroids were used on day 10. After culturing, the spheroids were washed with PBS and fixed with 10% formalin solution (Sigma) for 30 min. Then, spheroids were washed with Tris Buffered Saline (TBS) (Canvax Biotech) and permeabilized with 0.1% Triton X-100 (v/v) (Sigma) solution in TBS for 30 min, under agitation. Spheroids were blocked with 0.3% Triton X-100 (v/v) and 3% Donkey serum (v/v) (Sigma) into TBS for 2 h in shaking conditions. Spheroids were incubated overnight with primary antibody against mouse anti-insulin (1:500, Acris) in a blocking solution at 4 °C in shacking conditions. The following day, hydrogels were washed with permeabilization solution and incubated with secondary antibody

for 2 h at room temperature (Alexa-Fluor 647 conjugate goat anti-mouse 1:200) under agitation. DAPI (1:1000 Thermofisher) was used to stain nuclei. Finally, spheroids were washed with TBS for 15 min and stored at 4 °C until confocal microscopy acquisition. Images were taken using an LSM 800 from Zeiss.

Glucose-Stimulated Insulin Secretion (GSIS): Encapsulated spheroids were preincubated with Krebs-Ringer bicarbonate HEPES buffer solution at day 7 after fabrication (115×10^{-3} M NaCl, 24×10^{-3} M NaHCO₃, 5×10^{-3} M KCl, 1×10^{-3} M MgCa₂·6H₂O, 1×10^{-3} M CaCl₂·2H₂O, 20×10^{-3} M HEPES and 0.5% BSA, pH 7.4) containing 2.8×10^{-3} M glucose for 30 min. Three spheroids per condition were used for the GSIS study. Then, spheroids were incubated at low glucose (2.8×10^{-3} M) for 90 min, then incubated at high glucose (16.7×10^{-3} M) for 90 min. After each incubation, supernatants were collected, and cellular insulin contents were recovered in acid-ethanol solution. Insulin concentration was determined by ELISA (Crystal Chem).

Statistical Analysis: Results are expressed as mean values ± standard error of the mean (SEM), and all statistical analyses were performed using GraphPad Prism 8.3.0. One-way analysis of variance was performed followed by Dunnett's or Tukey's multiple comparison post hoc tests, to determine individual differences between the groups. The representation of statistical significance is as follows: * $p < 0.05$, ** $p < 0.01$, and *** $p < 0.001$, **** $p < 0.0001$.

Supporting Information

Supporting Information is available from the Wiley Online Library or from the author.

Acknowledgements

This project received financial support from the European Research Council program under grants ERC-StG-DAMOC (714317), H2020 EU framework FET-open BLOC (863037), the Spanish Ministry of Economy and Competitiveness, through the “Severo Ochoa” Program for Centres of Excellence in R&D (SEV-2020-2023), the CERCA Programme/ Generalitat de Catalunya (2017-SGR-1079) and Fundación Bancaria “la Caixa”- Obra Social “la Caixa” (project IBEC-La Caixa Health Ageing) to JR-A. PIT19/00896 integrated in the Plan Estatal de I+D+I and cofinanced by ISCIII-Subdirección General de Evaluación and Fondo Europeo de Desarrollo Regional (FEDER-“A way to build Europe”) to R.G. The raw/processed data required to reproduce these findings cannot be shared at this time as the data also forms part of an ongoing study.

Conflict of Interest

The authors declare no conflict of interest.

Authors Contributions

L.C.-F. and F.C. contributed to the study design, performance of experiments, data analysis, and writing and review of the manuscript. J.C. contributed to the performance of hydrogels micro-rheology analysis and A.G.-A to the in vivo experiment. J.R.-A. and R.G contributed to the study design, data analysis, and report and manuscript review. J.R.-A is the guarantor of this work. It had full access to all the data in the study and took responsibility for the data integrity and data analysis accuracy.

Data Availability Statement

The data that support the findings of this study are available from the corresponding author upon reasonable request.

Keywords

3D bioprinter, microspheres, encapsulation, collagen, β -cell

Received: December 21, 2021

Revised: January 18, 2022

Published online: February 20, 2022

- [1] P. D. Burbelo, E. E. Lebovitz, K. E. Bren, A. Bayat, S. Paviol, J. M. Wenzlau, K. J. Barriga, M. Rewers, D. M. Harlan, M. J. Iadarola, *PLoS One* **2012**, 7, 45216.
- [2] A. E. Ssson-noguera, J. Ciriza, A. Cañibano-hernández, R. Villa, L. Saenz, M. Alvarez, J. Luis, *Int. J. Pharm.* **2019**, 566, 604.
- [3] J. M. Chem, A. U. Ernst, L. Wang, M. Ma, L. Wang, *J. Mater. Chem. B* **2018**, 6, 6705.
- [4] S. T. Bartlett, J. F. Markmann, P. Johnson, O. Korsgren, B. J. Hering, D. Scharp, T. W. H. Kay, J. Bromberg, J. S. Odorico, G. C. Weir, N. Bridges, R. Kandaswamy, P. Stock, P. Friend, M. Gotoh, D. K. C. Cooper, *Report from IPITA-TTS Opinion Leaders Meeting on the Future of B-Cell Replacement*, **2016**.
- [5] A. Espona-noguera, J. Etxebarria-elezgarai, L. Saenz, A. Cañibano-hernández, H. Gurruchaga, F. J. Blanco, G. Orive, R. M. Hernández, *Int. J. Pharm.* **2019**, 560, 65.
- [6] G. A. P. Juárez, M. Spasojevic, M. M. Faas, P. de Vos, *Front. Bioeng. Biotechnol.* **2014**, <https://doi.org/10.3389/fbioe.2014.00026>.
- [7] A. J. Vegas, O. Veisoh, M. Gürtler, J. R. Millman, W. Felicia, A. R. Bader, J. C. Doloff, J. Li, M. Chen, H. H. Tam, S. Jhunjunwala, E. Langan, S. Aresta, S. Gandham, J. McGarrigle, M. A. Bochenek, J. Oberholzer, D. L. Greiner, G. C. Weir, D. A. Melton, R. Langer, D. G. Anderson, *Nat. Med.* **2016**, 22, 306.
- [8] J. M. Lee, D. Y. Park, L. Yang, E. Kim, C. D. Ahrberg, K. Lee, B. G. Chung, *Sci. Rep.* **2018**, 8, 17145.
- [9] K. Moshksayan, N. Kashaninejad, M. Ebrahimi, J. G. Lock, *Sens. Actuators, B* **2018**, 263, 151.
- [10] C. S. U., *Tissue Eng., Part C* **2017**, 23, 516.
- [11] D. Lee, C. Cha, *Pharmaceutics* **2018**, 10, 229.
- [12] J. M. Lee, J. W. Choi, C. D. Ahrberg, H. W. Choi, J. H. Ha, S. G. Mun, *Microsystems Nanoeng.* **2020**, 6, 52.
- [13] J. Crisóstomo, A. M. Pereira, S. J. Bidarra, A. C. Gonçalves, P. L. Granja, J. F. Coelho, C. C. Barrias, R. Seça, *J. Appl. Biomater. Funct. Mater.* **2019**, 17.
- [14] K. Y. Lee, D. J. Mooney, *Prog. Polym. Sci.* **2012**, 37, 106.
- [15] Y. Suzuki, Y. Nishimura, M. Tanihara, K. Suzuki, T. Nakamura, Y. Shimizu, Y. Yamawaki, Y. Kakimaru, *J. Biomed. Mater. Res.* **1998**, 39, 317.
- [16] J. K. Wang, N. Mein, J. Cheam, S. A. Irvine, N. S. Tan, S. Venkatraman, C. Y. Tay, *Macromol. Rapid Commun.* **2020**, 41, 2000275.
- [17] M. Riopel, S. Diego, R. Wang, *Front. Biosci.* **2014**, 19, 77.
- [18] T. B. Mckay, S. Priyadarsini, D. Karamichos, *Cells* **2019**, 8, 1239.
- [19] T. Narita, S. Yunoki, Y. Ohyabu, N. Yahagi, T. Uraoka, *Med. Devices: Evidence Res.* **2016**, 2016, 429.
- [20] I. D. Gaudet, D. I. Shreiber, *Biointerphases* **2012**, 7, 25.
- [21] D. Fortunati, D. Yi, S. Chau, Z. Wang, R. John, *Amino Acids* **2014**, 46, 1751.
- [22] P. Velmurugan, E. Ramaprasad, A. Singam, R. R. Jonnalagadda, V. Subramanian, *Biopolymers* **2013**, 101, 471.
- [23] J. Y. Lee, H. Lim, J. W. Ahn, D. Jang, S. H. Lee, K. Park, S. E. Kim, *Int. J. Mol. Sci.* **2018**, 19, https://www.mdpi.com/1422-0067/19/11/3602?type=check_update&version=1.
- [24] P. R. Shorten, C. D. McMahon, T. K. Soboleva, *Biophys. J.* **2007**, 93, 3001.
- [25] F. Krombach, S. Münzing, A. M. Allmeling, J. T. Gerlach, J. Behr, M. Dörger, *Environ. Health Perspect.* **1997**, 105, 1261.

- [26] H. Tasnim, G. M. Fricke, J. R. Byrum, J. O. Sotiris, J. L. Cannon, M. E. Moses, *Front. Immunol.* **2018**, <https://doi.org/10.3389/fimmu.2018.01571>.
- [27] J. P. PRIESTLE, H.-P. SCHÄR, M. G. GRÜTTER, *Biochem. Soc. Trans.* **1988**, *16*, 949.
- [28] H. Park, X. Guo, J. S. Temenoff, Y. Tabata, A. I. Caplan, F. K. Kasper, A. G. Mikos, *Biomacromolecules* **2010**, *10*, 541.
- [29] C. Y. Liu, M. Matsusaki, M. Akashi, *Polym. J.* **2015**, *47*, 391.
- [30] F. M. Cross, Sarah J. Linker, Kay E. Leslie, *Physiol. Behav.* **2016**, *176*, 100.
- [31] G. Huang, L. Wang, S. Wang, Y. Han, J. Wu, Q. Zhang, F. Xu, T. J. Lu, *Biofabrication* **2012**, *4*, 042001.
- [32] C. F. Guimarães, L. Gasperini, A. P. Marques, R. L. Reis, *Nat. Rev. Mater.* **2020**, *5*, 351.
- [33] D. E. Discher, P. Janmey, Y. L. Wang, *Science* **2005**, *310*, 1139.
- [34] A. Galli, M. Algerta, P. Marciiani, C. Schulte, C. Lenardi, P. Milani, E. Maffioli, G. Tedeschi, C. Perego, *Cells* **2020**, *9*, 413.
- [35] D. Liepsch, *J. Biomech.* **2016**, *35*, 415.
- [36] J. Lee, M. Yeo, W. Kim, Y. Koo, G. H. Kim, *Int. J. Biol. Macromol.* **2018**, *110*, 497.
- [37] L. Tjäderhane, F. D. Nascimento, L. Breschi, A. Mazzoni, I. L. S. Tersariol, S. Geraldini, A. Tezvergil-mutluay, M. R. Carrilho, R. M. Carvalho, F. R. Tay, D. H. Pashley, *Dent. Mater.* **2014**, *29*, 116.
- [38] C. Mura, C. Dissaux, K. Bouzakri, A. Lejay, C. Bruant-rodier, M. Pinget, E. Maillard, *Cell Transplant.* **2018**, *27*, 1289.
- [39] E. Kniazeva, A. J. Putnam, *Am. J. Physiol.* **2009**, *297*, C179.
- [40] and R. K. Daniel López, H. Vlamakis, R. Losick, *Bone* **2008**, *23*, 1.
- [41] N. G. Genes, J. A. Rowley, D. J. Mooney, L. J. Bonassar, *Arch. Biochem. Biophys.* **2004**, *422*, 161.
- [42] T. P. Kraehenbuehl, P. Zammaretti, A. J. Van der Vlies, R. G. Schoenmakers, M. P. Lutolf, M. E. Jaconi, J. A. Hubbell, *Biomaterials* **2008**, *29*, 2757.
- [43] K. S. Straley, S. C. Heilshorn, *Soft Matter* **2009**, *5*, 114.
- [44] A. Espona-Noguera, J. Ciriza, A. Cañibano-Hernández, G. Orive, R. M. Hernández, L. S. Del Burgo, J. L. Pedraz, *Pharmaceutics* **2019**, *11*, 597.
- [45] K. Hayashi, Y. Tabata, *Acta Biomater.* **2011**, *7*, 2797.
- [46] T. B. Lopez-Mendez, E. Santos-Vizcaino, J. L. Pedraz, G. Orive, R. M. Hernandez, *J. Controlled Release* **2021**, *335*, 619.
- [47] G. Cidonio, M. Glinka, J. I. Dawson, R. O. C. Oreffo, *Biomaterials* **2019**, *209*, 10.
- [48] S. W. Attwood, *J. Clin. Med.* **2019**, *8*, 288.
- [49] H. Shahjalal, A. A. Dayem, K. M. Lim, T. Jeon, S. Cho, *Stem Cell Res.* **2018**, *9*, 355.
- [50] L. M. Weber, K. N. Hayda, K. S. Anseth, *Tissue Eng., Part A* **2008**, *14*, 1959.